CELLIANT®

Powered by You

Infrared Radiative Properties and Thermal Modeling of Ceramic Embedded Textile Fabrics

Dr. David Anderson, John Fessler, Matthew Pooley, Scott Seidel, Dr. Michael Hamblin, Haskell Beckham and Dr. James F Brennan

Infrared radiative properties and thermal modeling of ceramic-embedded textile fabrics

DAVID M. ANDERSON,[1]* JOHN R. FESSLER,[2] MATTHEW A. POOLEY,[3] SCOTT SEIDEL,[1] MICHAEL R. HAMBLIN,[4] HASKELL W. BECKHAM,[1] AND JAMES F. BRENNAN, III[1]

[1] *Exponent, Inc., 3350 Peachtree Road NE, Suite 1125, Atlanta, GA 30326 USA*
[2] *Exponent, Inc., 15615 Alton Parkway, Suite 350, Irvine, CA 92618 USA*
[3] *Exponent, Inc., 420 Lexington Avenue, Suite 1740, New York, NY 10170 USA*
[4] *Wellman Center for Photomedicine, Harvard Medical School, 50 Blossom Street, Boston, MA 02114 USA*

*danderson@exponent.com

Abstract: The infrared optical properties of textiles are of great importance in numerous applications, including infrared therapy and body thermoregulation. Tuning the spectral response of fabrics by engineering of composite textile materials can produce fabrics targeted for use in these applications. We present spectroscopic data for engineered polyester fabric containing varying amounts of ceramic microparticles within the fiber core and report a spectrally-dependent shift in infrared reflectance, transmittance and absorptance. A thermal transport model is subsequently implemented to study the effect of these modified properties on the spectral distribution of infrared radiation incident upon the wearer of a garment constructed of this fabric.

OCIS codes: (300.6340) Spectroscopy, infrared; (110.3175) Infrared imaging; (120.6810) Thermal effects.

References and links

1. S. B. Warner, *Fiber Science* (Prentice Hall, 1995) pp. 213-229.
2. US Patent, No: 5344297 (1994).
3. M.A. Pooley, D.M. Anderson, H.W. Beckham and J.F. Brennan III , "Engineered emissivity of textile fabrics by the inclusion of ceramic particles," Opt. Express **24**(10), 10556–10564 (2016).
4. W.W. Carr, D.S. Sarma, M.R. Johnson, B.T. Do and V.A. Williamson. "Infrared absorption studies of fabrics," Textile Res. J. **67**(10) 725-738 (1997).
5. P. Hsu, A.Y. Song, P.B. Catrysse, C. Liu, Y. Peng, J. Xie, S. Fan and Y. Cui, "Radiative human body cooling by nanoporous polyethylene textile," Science **353**(6303), 1019-1023 (2016).
6. F. Vatansever and M.R. Hamblin, "Far infrared radiation (FIR): its biological effects and medical applications," Photonics Lasers Med. **1**(4), 255-266 (2012).
7. J.D. Hardy and E.F. DuBois, "Regulation of heat loss from the human body," Proc. Nat. Acad. Sci. **23**(12), 624-631 (1937).
8. C.-E. A. Winslow, A.P. Gagge and L.P. Harrison, "The influence of air movement upon heat losses from the clothed human body," Am. J. Physiol. **127**(3) 508-515 (1939).
9. ASTM E408-13, *Standard Test Methods for Total Normal Emittance of Surfaces Using Inspection-Meter Techniques,* (ASTM International, 2013).
10. F.P. Incropera and D.P. Dewitt, *Fundamentals of Heat and Mass Transfer, 5th Ed.* (John Wiley & Sons, 2002).
11. G. Nellis and S. Klein, *Heat Transfer* (Cambridge University Press, 1997).
12. E.A. Arens and H. Zhang, "The skin's role in human thermoregulation and comfort" in *Thermal and moisture transport in fibrous materials*, N. Pan and P. Gibson, Eds. (Woodhead Publishing Limited, 2006).
13. ASTM G173-03, *Spectral Solar Irradiance,* (ASTM International, 2003).
14. A.C. Guyton and J.E. Hall, *Textbook of Medical Physiology* (W.B. Saunders Company, 2000).

1. Introduction

The engineering of textiles to exhibit desired optical properties has long been explored, with success demonstrated in various methods including: co-spinning of different materials,

introduction of gradients in fiber cross-sectional shape, inclusion of inorganic content, or use of dyes and other additives [1,2]. Recently, increased attention has been paid to the interactions between textile products and infrared radiation, due to the potential impact in applications ranging from body cooling to industrial drying processes to infrared therapy [3–6]. Mid-infrared optical properties are of particular importance when considering interactions with the human body, as at nominal skin temperature much of the body's emissive radiative power is centered in the mid-infrared between 7 and 14 μm, and infrared heat losses account for approximately 50% of body cooling in typical indoor conditions [7,8].

In the work presented herein, we utilized Fourier transform infrared (FTIR) spectroscopy to assess the spectral optical properties – namely the near-normal reflectance, transmittance, and emittance – of textile fabrics knitted with varying percentages of ceramic-bearing polymeric fibers. The biological effects of garments manufactured from these fabrics are presently under investigation [6]. The fabrics, which we also studied in our previous work [3], were nominally identical in thickness, basis weight, knit structure, and color. All fabrics consisted of 8% elastane fibers and 92% polyethylene terephthalate (PET, i.e., polyester) based fibers; the only difference between the samples was the fraction of these fibers that contained a core of polyester blended with ceramic particles (e.g., titanium dioxide) for optical property modification.

The measured optical properties were subsequently utilized in a first-principle-based heat transfer model, accounting for emitted, reflected and transmitted radiant energy as well as thermal transport via conduction and convection, to determine the magnitude and spectral distribution of infrared energy received by a wearer of each fabric in the 0.8 – 16.7 μm spectral region. It is demonstrated that with increasing added ceramic content, the modified textile fabrics reflect and transmit less infrared energy and thus absorb more. This is particularly evident at wavelengths shorter than 6 μm. As a result, the modified fabrics with added ceramic content can absorb incoming radiation from the sun in the near-IR region, and emit increased levels of infrared energy at longer wavelengths, as compared to the same fabric without ceramic content. Thermal modeling indicates that this effect persists over a broad range of environmental and fit factors; such a fabric could be utilized when the physical properties of a polyester blend warrant its selection over alternative fabric materials, yet modified near- and mid-infrared optical properties are desired.

2. Experimental Methods

A Nicolet iS50 FTIR spectrometer (Thermo-Fisher Scientific) was used to measure the spectral reflectance (ρ_λ) and transmittance (τ_λ) of the fabric samples with differing percentages of ceramic-bearing fibers. Because of the diffuse nature of reflection and transmission from composite surfaces [9], a mid-IR IntegratIR^{TM} integrating sphere (Pike Technologies) with a reflective gold inner coating and a deuterated triglycine sulfate detector was used to measure the reflected or transmitted infrared radiation from the fabric samples. Mid-IR measurements were conducted across a wavenumber range of 4000 – 600 cm^{-1} (corresponding to wavelengths, λ, ranging from 2.5 – 16.7 μm), using a potassium bromide (KBr) beam splitter. Near-IR measurements, ranging from wavenumbers of 12000 – 4000 cm^{-1} ($0.8 < \lambda < 2.5$ μm) were conducted using a near-IR Nicolet iS50 NIR integrating sphere module (Thermo-Fisher Scientific) with an indium gallium arsenide detector.

A schematic of the FTIR setup, indicating the sample placement relative to the IR source and detector for the various reflectance and transmittance measurements is shown in Fig. 1.

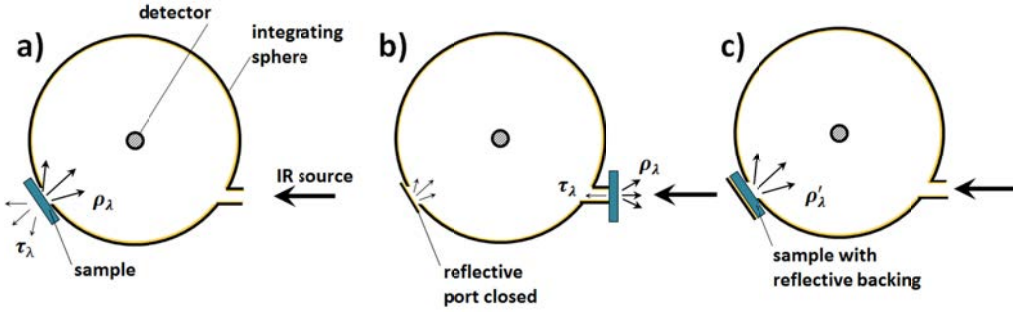

Fig. 1. Schematic illustrating an FTIR setup for measurement of a) direct reflectance, b) direct transmittance, and c) indirect transmittance via change in reflectance

Because the near-IR integrating sphere did not allow placement of the sample directly between the IR source and the sphere inlet, the transmittance was instead assessed indirectly by comparing the reflectance where transmitted IR was permitted to escape through the sample (ρ_λ) to the reflectance with a reflective backing behind the sample (ρ'_λ). The spectral transmittance can be shown to be related to the ρ_λ and ρ'_λ reflective measurements illustrated in Fig. 1(a) and Fig. 1(c), respectively, by:

$$\tau_\lambda = \left[\frac{\rho'_\lambda - \rho_\lambda}{1 + \sum_{j=1}^{\infty} \rho_\lambda^j} \right]^{1/2} \tag{1}$$

Details of this relationship are included in the Appendix. The methodology of calculating transmittance from the reflectance measurements with and without a 100% reflective backing was validated through comparison of indirect to direct transmittance measurements with the mid-IR integrating sphere setup where such direct measurement was possible.

To minimize the effect of absorption by water vapor and other trace gas compounds, the integrating sphere was surrounded with desiccant and the interior was swept with 5 scfh (standard cubic feet per hour) of inert nitrogen gas during all measurements.

Four different fabric samples were examined, each containing 0, 0.82, 0.91 or 1.18 weight percent inorganic content from modified ceramic-bearing fibers. For each fabric sample, absorption and transmission spectra were calculated by averaging the respective spectra measured for 5 unique specimens. For each specimen, the absorption and transmission spectra were obtained from 256 scans at a resolution of 16 cm^{-1}.

3. Experimental Results

The results of the FTIR measurements are reported in this section. Although reflectance and transmittance are often used interchangeably with reflectivity and transmissivity, respectively, the terminology ending in '-ance' is used in this paper to note that textiles are a mixture of fibers and air, and not pure substances. Because radiation properties such as reflectance and transmittance of non-conducting materials such as textiles do not vary for incidence angles less than 70° from normal [10], the values measured according to the schematic shown in Fig. 1 are reported as near-normal properties.

While not directly measured, the spectral absorptance (α_λ) of each fabric can be determined because the reflectance, transmittance and absorptance must sum to unity ($\rho_\lambda + \tau_\lambda + \alpha_\lambda = 1$). Also, according to Kirchoff's law, the spectral near-normal emittance (ε_λ) must equal the near-normal absorptance [10].

3.1 Mid-IR reflectance, transmittance and emittance

The spectral mid-IR properties of the textile samples are shown in Fig. 2. The most significant difference between the various fabrics appears in wavenumbers greater than approximately 1700 cm^{-1} (wavelengths below 6 μm). Each of the fabric samples exhibit similar overall spectral patterns, with a series of narrow absorption peaks between 3000 – 2000 cm^{-1} wavenumbers. Increasing amounts of ceramic content, however, generally decreases the reflectance and transmittance, and increases absorptance, in the 4000 – 2000 cm^{-1} region. Similar behavior occurs at smaller wavenumbers; however, the effect is less pronounced because the overall absorptance is already high at these longer wavelengths.

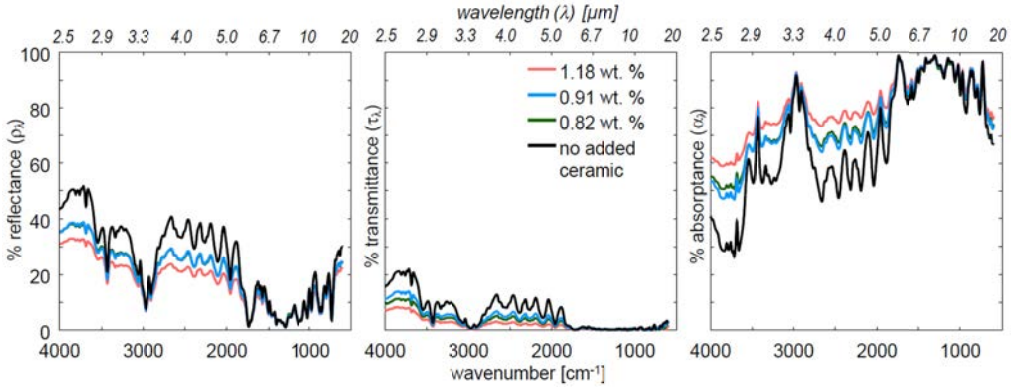

Fig. 2. Spectral reflectance (ρ_λ), transmittance (τ_λ), and absorptance (α_λ) in the mid-IR region for knit textile fabrics consisting of varying wt. % of ceramic contained in the fiber cores. All plots have a common y-scale ranging from 0-100%.

To better illustrate how the optical properties align with infrared radiation emitted by the human body, Fig. 3 plots these properties as a function of wavelength, as opposed to wavenumber, for the fabric with the maximum amount of added ceramic (1.18 wt. %) and with no added ceramic. The figure also illustrates the spectral distribution of intensity of radiation emitted by a blackbody at a nominal skin temperature of 35°C. This emission is described by Planck's distribution:

$$E_b(\lambda,T)=\frac{C_1}{\lambda^5\left[e^{C_2/\lambda T}-1\right]} \tag{2}$$

where the first and second radiation constants are $C_1 = 3.742 \times 10^8$ W·μm^4/m^2 and $C_2 = 1.439 \times 10^4$ μm^4·K, respectively [10].

As can readily be seen in Fig. 3, the spectral region where the impact of added ceramic is greatest ($\lambda < 6$ μm) corresponds to an area with less significant magnitude of radiation at nominal body temperature; less than 5% of the total radiation of a blackbody at 35°C is contained in this region [10]. To provide a representative value for an optical property, it must be spectrally weighted by its source of radiation. For example, the average reflectance over a wavelength range of λ_1-λ_2 is:

$$\overline{\rho}_{\lambda_1-\lambda_2}=\frac{\int \rho_\lambda \cdot E_b(\lambda,T)\cdot d\lambda}{\int E_b(\lambda,T)\cdot d\lambda} \tag{3}$$

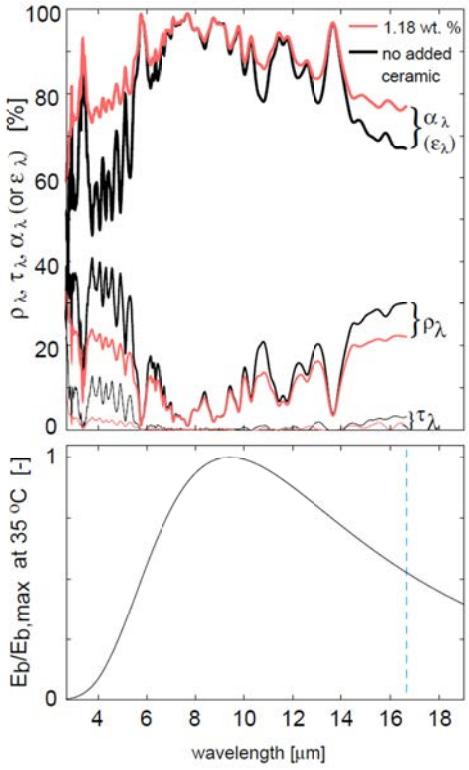

Fig. 3. (Top) Spectral optical properties of the fabric samples containing the maximum (1.18 wt. %) and minimum (0 wt. %) added ceramic content. (Bottom) Normalized Planck's distribution for a blackbody at 35°C.

Similarly, the average spectral transmittance and absorptance/emittance are given by:

$$\overline{\tau}_{\lambda_1-\lambda_2} = \frac{\int \tau_\lambda \cdot E_b(\lambda,T) \cdot d\lambda}{\int E_b(\lambda,T) \cdot d\lambda} \tag{4}$$

$$\overline{\varepsilon}_{\lambda_1-\lambda_2} = \overline{\alpha}_{\lambda_1-\lambda_2} = \frac{\int \alpha_\lambda \cdot E_b(\lambda,T) \cdot d\lambda}{\int E_b(\lambda,T) \cdot d\lambda} \tag{5}$$

In our prior study we used an IR camera, with spectral sensitivity between 7.5 – 14 μm, to investigate the same four fabrics considered herein, and found a statistically significant trend of increasing emittance with increasing added ceramic content [3]. The FTIR emittance and absorptance results in Fig. 2 and Fig. 3 can be weighted by the source power distribution for a wider wavelength range. The emittance values measured via FTIR in the present work agree well with the prior IR camera measurements (i.e., Pooley, et al.) for the 7.5 – 14 μm spectral range used in that study; the slope of the ceramic content vs. emittance linear best fit curve in Fig. 4 matches between measurement techniques. Moreover, while the absolute values of emittance are slightly lower when assessed by the FTIR, the differences are within the experimental error bars.

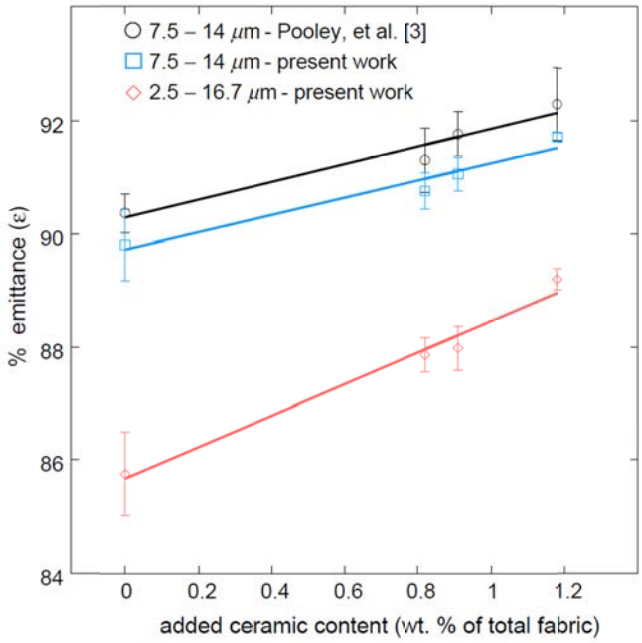

Fig. 4. Emittance of the fabric samples as a function of added ceramic material. Data points for the present work represent the mean of spectrally averaged emittance values from five independent samples. Two separate spectral ranges – 7.5-14 μm to match the detection range of the IR camera and the entire 2.5-16.7 μm measurement range – are utilized to calculate average emittance values.

When the broader 2.5 – 16.7 μm mid-IR spectral range is considered, the impact of added ceramic content on emittance is even greater, as evidenced by the steeper gradient for this wavelength range in Fig. 4, due to the more significant difference in properties where $\lambda < 6$ μm. Table 1 summarizes the spectral average mid-IR properties of the four fabric samples with varying wt. % added ceramic content. It should be noted that the wt. % values reported in our prior study [3] did not account for the inorganic additive present in standard polyester; hence the values reported in Table 1 vary slightly from what was previously reported for the same samples. However, these slight variations do not affect the conclusions from that study, which remain unchanged.

Table 1. Spectral average mid-IR optical properties at 35°C (2.5 – 16.7 μm)

Sample No.	Wt. % ceramic from modified fibers[a]	Transmittance [%]	Reflectance [%]	Emittance [%]
1	1.18	0.34 +/- 0.19	10.5 +/- 0.2	89.2 +/- 0.2
2	0.91	0.68 +/- 0.21	11.3 +/- 0.3	88.0 +/- 0.4
3	0.82	0.53 +/- 0.10	11.6 +/- 0.3	87.9 +/- 0.3
4	0	0.92 +/- 0.15	13.3 +/- 0.8	85.8 +/- 0.7

[a] Calculated from the ratio of the ceramic mass contained in the modified fibers to the overall mass of the fabric, using ash-content data collected using ASTM D5630. The ceramic content in standard polyester was determined from the fabric sample that did not contain added ceramics (Sample 4).

3.2 Near-IR reflectance, transmittance and emittance

At its relatively modest temperature, the human body does not emit significant radiation at near-IR wavelengths; however, optical properties in this region are of interest due to

interactions with radiation from hotter sources (most notably, the sun). The reflectance and transmittance of the fabric samples in the near-IR region are shown in Fig. 5.

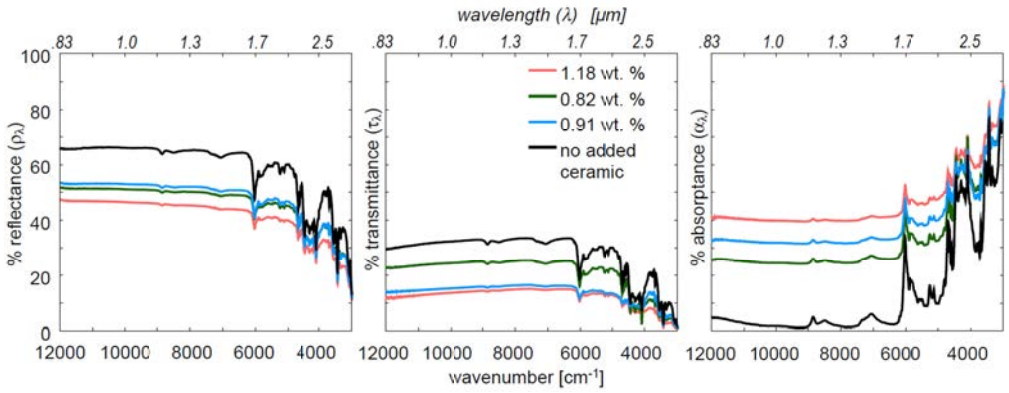

Fig. 5. Near-IR spectral reflectance (ρ_λ), transmittance (τ_λ), and absorptance (α_λ) of the knit textile fabrics. Spectral data down to 3000 cm^{-1} are included; the data for wavenumbers from 3000 – 4000 cm^{-1} were collected using the mid-IR integrating sphere, illustrating that the data are continuous and consistent between setups and regardless of whether the direct or indirect approach was utilized to measure transmittance.

The fabric with no added ceramic exhibits significantly higher reflectance and transmittance, and therefore lower absorptance, than fabrics that do contain fibers impregnated with ceramic particles. The magnitude of the impact on ceramic content in the near-IR region is even more significant than the impact in the mid-IR region shown in Fig. 2; this will have significant impact on the solar radiation absorbed by and transmitted through the fabric, as approximately 50% of the solar spectrum falls in the near-IR region [11].

4. Impact of optical properties on infrared irradiation received by body

4.1 Heat transfer model

To understand the impact of the change in radiative optical properties on the wearer of a fabric, an energy-conservation-based heat transfer model was developed. This model accounts for all possible modes of radiative interaction – reflection, absorption, and transmission – between the body, fabric and environment, as well as non-radiative heat transfer via conduction and convection. The fabric is modeled as being in instantaneous thermal equilibrium with its surroundings. The ambient surroundings are approximated as being sufficiently large relative to the fabric surface such that radiation is exchanged with the fabric as if the surroundings behave like a blackbody at T_{amb}. The fabric is assumed to be sufficiently thin such that its temperature is uniform and cross-fabric thermal gradients can be neglected. Evaporative cooling is neglected in the model, as the goal of the model is to compare the relative radiative heat transfer rates for fabrics with different ceramic contents, and evaporative cooling is expected to be relatively independent of this effect [12]. Under these assumptions, the skin-fabric-environment system and pertinent mechanisms of heat exchange are shown in Fig. 6.

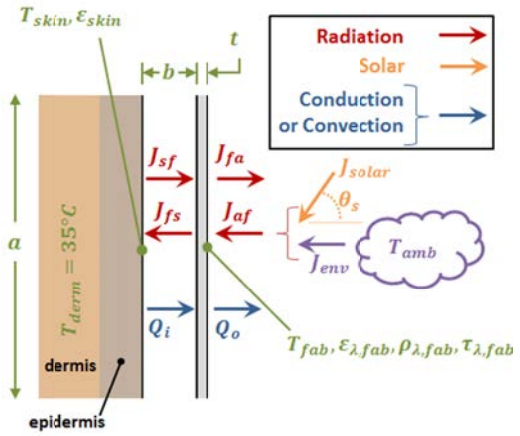

Fig. 6. Fabric geometry and relevant modes of heat transfer

Each radiative heat flux component, shown in red, includes reflected and transmitted radiation in addition to emitted radiation (i.e., it represents a radiosity [10]). Radiative energy is transferred from the skin to the fabric (J_{sf}), the fabric to the skin (J_{fs}), the fabric to the ambient surroundings (J_{fa}), and from the ambient surroundings to the fabric (J_{af}). The radiative heat flux from the surroundings can include both solar irradiation (J_{solar}) and irradiation from the surroundings (J_{env}) at ambient temperature (T_{amb}). The non-radiative heat fluxes due to convection and/or conduction (Q_i and Q_o) are shown in blue. The fabric of thickness t is located between the wearer (at temperature T_{skin}) and the surroundings (at T_{amb}) and is separated from the wearer's skin by a gap of b thickness.

At steady state, the energy conservation on the fabric can be represented, on a per unit area basis [W/m^2] by:

$$(J_{sf} + Q_i + J_{af}) - (J_{fs} + J_{fa} + Q_o) = 0 \tag{6}$$

The general form of the non-radiative heat fluxes is $Q = h_{eff} \cdot (T_{surface} - T_{surroundings})$ where h_{eff} is the average convective heat transfer coefficient and is a function of the geometry and flow characteristics. Conduction across the air gap for Q_i is a special case of $h_{eff} = k_{air}/b$, where k_{air} is the thermal conductivity of air, that occurs when the gap b is sufficiently small such that viscous forces damp out buoyancy effects [10,11]. It is important to note that in the case of $T_{amb} > T_{fab}$, the direction of heat transfer will change; however, this is accounted for appropriately in the model (i.e., Q_o and Q_i will be negative, indicating heat flow in the opposite direction of the arrow shown in Fig. 6). The total radiative fluxes (represented by uppercase J's in Fig. 6) are determined by integrating the spectral flux, or the radiative heat flux leaving surface x in the direction of surface y is $J_{xy} = \int j_{xy}(\lambda) \cdot d\lambda$. Similarly, the solar irradiation is determined by integrating the spectral solar intensity normal to the fabric surface, or $J_{solar} = \int j_{solar}(\lambda) \cdot \cos(\theta_s) \cdot d\lambda$. The spectral solar intensity, accounting for atmospheric transmission losses, is taken from ASTM G-173 [13].

The spectral radiative heat flux leaving each surface has a component of emission, reflection, and transmission and can be written as:

$$j_{af}(\lambda) = E_b(\lambda, T_{amb}) + j_{solar}(\lambda) \cdot \cos(\theta_s) \tag{7}$$

$$j_{fa}(\lambda) = \varepsilon_{\lambda,fab} \cdot E_b(\lambda, T_{amb}) + \rho_{\lambda,fab} \cdot j_{af}(\lambda) + \tau_{\lambda,fab} \cdot j_{sf}(\lambda) \tag{8}$$

$$j_{sf}(\lambda) = \varepsilon_{skin} \cdot E_b(\lambda, T_{skin}) + \rho_{skin} \cdot j_{fs}(\lambda) \tag{9}$$

$$j_{fs}(\lambda) = \varepsilon_{\lambda,fab} \cdot E_b(\lambda, T_{fab}) + \rho_{\lambda,fab} \cdot j_{sf}(\lambda) + \tau_{\lambda,fab} \cdot j_{af}(\lambda) \tag{10}$$

Equations (8) - (10) are circularly defined with dependence upon one another. They are made independent by substituting Eq. (10) into Eq. (9) and solving explicitly for $j_{sf}(\lambda)$:

$$j_{sf}(\lambda) = \frac{\varepsilon_{skin} \cdot E_b(\lambda, T_{skin}) + \rho_{skin} \cdot \left[\varepsilon_{\lambda,fab} \cdot E_b(\lambda, T_{fab}) + \tau_{\lambda,fab} \cdot j_{af}(\lambda) \right]}{1 - \rho_{skin} \cdot \rho_{\lambda,fab}} \tag{11}$$

An iterative solution procedure can be used to solve for the required fabric temperature to satisfy the energy balance given in Eq. (6). The specific heat transfer correlations used to determine the effective heat transfer coefficients in determining the non-radiative heat transfer components Q_i and Q_o, as well as the procedure for adjusting the epidermis skin temperature based on the external heat transfer rate, can be found in the Appendix.

4.2 Spectral shift in incident infrared radiation to the body

Of interest for therapeutic applications is the magnitude and spectral distribution of radiation received by the body as a result of wearing a fabric, namely $j_{fs}(\lambda)$ given by Eq. (10). A common set of baseline input parameters, provided in Table 2, are used in the thermal model. The fabric gap, ambient temperature, air velocity and solar incidence angle can all be adjusted in the model to evaluate sensitivity to these environmental and fit factors.

Table 2. Thermal model simulation parameters

Property	Value	Notes
dermis temp (T_{derm})	35°C	regulated by vasoconstriction/vasodilation [12]
skin emittance (ε_{skin})	0.98	greybody, opaque ($\rho_{skin} = 1 - \varepsilon_{skin}$) [10]
height (a)	0.3 m	estimate of torso dimensions [12]
width (w)	0.3 m	estimate of torso dimensions [12]
fabric gap (b)	5 mm	adjustable parameter
ambient temp (T_{amb})	23°C	adjustable parameter
air velocity (v)	1 m/s	adjustable parameter
solar angle (θ_s)	45°	adjustable parameter

Under the baseline conditions of Table 2, Fig. 7 shows the resulting spectral distribution of infrared radiation incident on the skin $j_{fs}(\lambda)$ for the fabrics with the maximum (1.18 wt. %) and minimum (0 wt. %) added ceramic content.

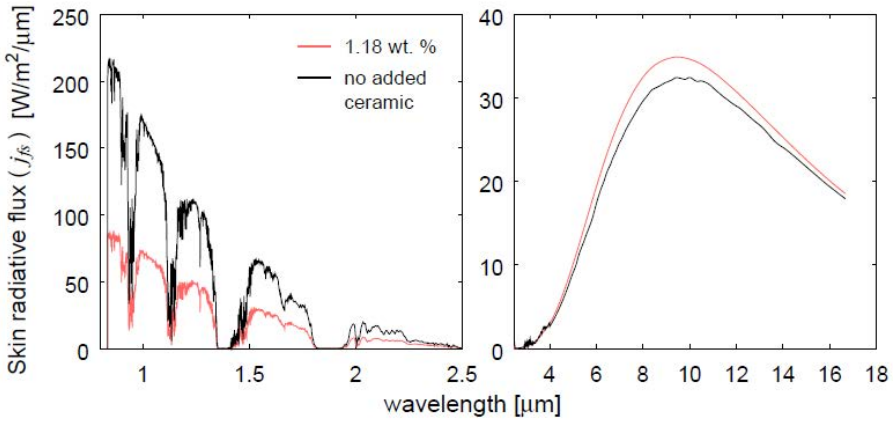

Fig. 7. Comparison of spectral distribution of infrared radiation received by the skin in the near-IR (left) and mid-IR (right) regions for the maximum (1.18 wt. %) and minimum (0 wt. %) added ceramic content fabric.

In the near-IR spectrum, the body will receive more infrared when wearing a garment composed of fabric with no added ceramic, due to the higher transmittance in this spectral region relative to the fabric with added ceramic. In contrast, the fabric with 1.18 wt. % added ceramic is able to absorb more of this solar near-IR radiation which is then re-emitted by the fabric at longer wavelengths. This shift in spectral incident radiation can be seen in the mid-IR portion of Fig. 7, where there is an increase in j_{fs} for wavelengths greater than 4 μm.

To determine if the increase in incident mid-IR radiation persists over a variety of environmental and fit factors, the model was run at different skin-fabric gap distances, ambient temperatures, wind speeds, and incident solar angles. The results of these simulations, used to calculate the total incident radiation in the mid-IR spectrum from 2.5 – 16.7 μm by integrating over this wavelength region for both the 0 wt. % and 1.18 wt. % added ceramic fabrics, are reported in Table 3. For the baseline case, all model input parameters match those listed in Table 2. For the other cases, only the parameter noted is changed from the baseline; the other parameters are held at the baseline state.

Table 3. Infrared radiation (2.5 – 16.7 μm) received by skin under various environmental and fit conditions

		Mid-IR Power [mW/cm^2]		
Parameter	Value	0 wt. %	1.18 wt. %	Δ
——— baseline ———		30.7	32.6	1.9
fabric gap (b)	10 mm	30.3	32.5	2.2
	1.0 mm	31.8	32.8	1.0
ambient temp (T_{amb})	30 °C	32.4	34.4	2.1
	10 °C	27.7	29.4	1.8
air velocity (v)	3.0 m/s	30.1	31.6	1.5
	0.1 m/s	31.3	33.6	2.4
solar angle (θ_s)	70°	30.4	31.3	0.9
	20°	30.8	33.4	2.6

Table 3 illustrates that the spectral shift in incident radiation to the wearer of a ceramic-embedded garment to the mid-IR region is present under a variety of scenarios. The incidence angle of solar irradiation appears to have the most significant effect on the magnitude of the shift; a similar effect to a less-normal incidence angle would be expected for cloudy days where the intensity of solar irradiation is reduced.

Increased solar absorption and subsequent re-emission of energy at longer wavelengths may be beneficial in numerous textile applications. The impacts of infrared radiation consisting of wavelengths ranging from 3 – 12 μm on tissue oxygenation and cell stimulation are under investigation [6]. Additionally, performance thermal outerwear designed for cold-weather applications could benefit from additional absorption from the solar spectrum to warm the outer surface of the garment and provide this heat to the wearer of the garment. Experimental studies of such ceramic-modified garments incorporating the use of thermal manikins or similar techniques should be conducted to assess these potential applications.

In summary, this study employed spectrophotometric measurements of textile fabrics modified with ceramic particles, finding favorable agreement with prior measurements using a scientific grade infrared camera on such fabrics. The increase in absorptance and emittance was mainly found to be focused in wavelengths below 6 μm, below the typical wavelength of human body radiation. However, in applications where the fabric receives radiation in this near-IR spectral region (e.g., via sunlight), thermal modeling indicates that the wearer will receive increased infrared radiation at wavelengths in the mid-IR (2.5 – 16.7 μm) portion of the electromagnetic spectrum, encompassing the wavelengths of human body radiation.

Acknowledgments
Partial funding for this work was provided by Hologenix, LLC (Santa Monica, CA). We thank Prof. Andrei Fedorov (Georgia Institute of Technology, Atlanta, GA) for insightful discussions regarding the heat transfer modeling of radiative energy exchange.

Appendix

A.1 Mathematical relationship to determine reflectance through the indirect method

Equation (1) shows the mathematical relationship between the spectral reflectivity with (ρ'_λ) and without (ρ_λ) a reflective backing (cf. Fig. 1). This relationship can be derived by considering the additional radiation reflected by the sample when a highly reflective backing is present, as shown in Fig. A-1.

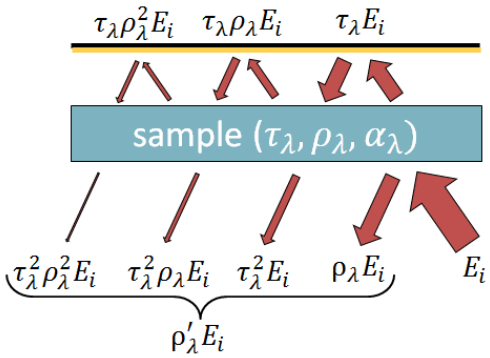

Fig. A-1. Reflection from a semi-transparent sample with reflective backing.

From Fig. A-1, it can readily be seen that:

$$\rho'_\lambda = \rho_\lambda + \tau_\lambda^2\left[1 + \rho_\lambda + \rho_\lambda^2 + \ldots\right] \tag{A.1}$$

Because the reflectivity must be less than 1, each term inside the brackets moving rightward becomes increasingly smaller, and Eq. (A.1) can be rewritten as:

$$\rho'_\lambda = \rho_\lambda + \tau_\lambda^2\left[1 + \sum_{j=1}^{\infty}\rho_\lambda^j\right] \tag{A.2}$$

A.2 Heat transfer correlations for non-radiative thermal transport coefficients

The general form of the convection heat flux (units, W/m^2) from a surface to its surrounding medium is given by Newton's law of cooling:

$$Q = \bar{h}\cdot\left(T_{surface} - T_{surroundings}\right) \tag{A.3}$$

where $\bar{h}$ is the average convective heat transfer coefficient, which is a function of the geometry and external flow characteristics [10]. Dimensionless variables describing the flow and geometry, such as the Reynolds number (Re_L) and/or Grashof number (Gr_L) are first calculated to understand the characteristics of the heat and momentum transfer, and along with the fluid's Prandtl number (Pr) these values are used to calculate an average dimensionless heat transfer coefficient ($Nu = f(Re_L, Gr_L, Pr)$). The dimensional average heat

transfer coefficient $\bar{h}$ is then the Nusselt number multiplied by the characteristic length (L_c) divided by the fluid thermal conductivity $\left(\bar{h} = Nu \cdot L_c \big/ k_{fluid}\right)$ [10,11].

In certain geometries, such as the gap between two parallel plates at different temperatures (i.e., between the skin and fabric), Eq. (A.3) can be employed regardless of whether conduction or convection is the dominant mode of heat transfer. If dimensionless analysis indicates that viscous dissipation forces outweigh the buoyancy forces generated by local differences in fluid density, conduction will prevail over convection and the Nusselt number will become unity (when $Nu = 1 = \bar{h} \cdot L_c / k_{fluid}$, it follows that $\bar{h} = k_{fluid} / L_c$, where the characteristic length L_c is the width of the gap between the plates). It can readily be seen that in this scenario, Eq. (A.3) becomes $Q = \bar{h} \cdot \Delta T = k_{fluid} \cdot \Delta T / L_c$ which is simply Fourier's law for steady-state one-dimensional conduction through a solid of uniform thermal conductivity.

A.2.1 Outer convection heat transfer coefficient

Convective heat transfer from the fabric to the ambient surroundings can occur by forced convection (resulting from external flow, such as wind, with a "free stream" velocity u_∞), free convection (driven by local buoyancy differences induced by a temperature gradient), or a combination of both. To determine which of these (or both) is significant; the Reynolds and Grashof numbers must be calculated [10,11].

$$\mathrm{Re}_L = \frac{\rho u_\infty L_c}{\mu} \tag{A.4}$$

$$Gr_L = \frac{g L_c^3 \beta \left| T_{amb} - T_{fab} \right|}{\nu^2} \tag{A.5}$$

where ρ is the fluid density, L_c is the characteristic length (in this case, the width of the plate w in Table 2), μ is the dynamic viscosity of the fluid, g is acceleration due to gravity, β is the coefficient of thermal expansion (reciprocal of absolute temperature for an ideal gas), and ν is the kinematic viscosity (ν=μ/ρ). All fluid properties are evaluated at the "film temperature," or the average of the fabric and ambient temperature. Three scenarios are possible and must be considered in estimating the average convective heat transfer coefficient:

1. The wind velocity u_∞ is sufficiently high for forced convection to dominate natural (free) convection. This is the case when $Gr_L/Re_L^2 \ll 1$. If $Gr_L/Re_L^2 < 0.1$, the average Nusselt number should be calculated based on forced convection correlations. If the Reynolds number is less than the critical Reynolds number of $Re_{crit} = 5.5\times10^5$, the flow is laminar and Eq. (A.6) applies. If not, the flow is turbulent and Eq. (A.7) is used [11].

$$Nu_{fc} = \frac{0.6674 Pr^{1/3} Re_L^{1/2}}{\left[1 + \left(0.0468 / Pr\right)^{2/3}\right]^{1/4}} \tag{A.6}$$

$$Nu_{fc} = \frac{0.6674 Pr^{1/3} Re_{crit}^{1/2}}{\left[1 + \left(0.0468 / Pr\right)^{2/3}\right]^{1/4}} + 0.037 Pr^{1/3} \left(Re_L^{0.8} - Re_{crit}^{0.8} \right) \tag{A.7}$$

2. In cases where the wind velocity is low, natural convection may dominate forced convection ($Gr_L/Re_L^2 \gg 1$). If $Gr_L/Re_L^2 > 10$, the dimensionless Rayleigh number ($Ra_L = Gr_L \cdot Pr$) must be calculated and used to determine the average Nusselt

number from natural convection correlations. The Rayleigh number is first used to calculate both the laminar and turbulent Nusselt numbers [11].

$$Nu_{nc,lam} = \frac{2.0}{\ln\left[1 + 2.0 \Big/ \left(C_{lam} \cdot Ra_L^{1/4}\right)\right]} \tag{A.8}$$

$$Nu_{nc,turb} = \frac{C_{turb,V} \cdot Ra_L^{1/3}}{1 + \left(1.4 \times 10^9\right) \cdot Pr / Ra_L} \tag{A.9}$$

where C_{lam} and $C_{turb,V}$ are dimensionless parameters given by:

$$C_{lam} = \frac{0.671}{\left[1 + \left(0.492 / Pr\right)^{9/16}\right]^{4/9}} \tag{A.10}$$

$$C_{turb,V} = \frac{0.13 \cdot Pr^{0.22}}{\left[1 + 0.61 \cdot Pr^{0.81}\right]^{0.42}} \tag{A.11}$$

The average Nusselt number can then be determined by asymptotically averaging the laminar and turbulent Nusselt numbers through the following empirical formula:

$$Nu_{nc} = \left[\left(Nu_{nc,lam}\right)^6 + \left(Nu_{nc,turb}\right)^6\right]^{1/6} \tag{A.12}$$

3. If the Grashof number is of the same order of magnitude as the square of the Reynolds number ($0.1 < Gr_L/Re_L^2 < 10$), the average Nusselt number can be determined by asymptotically averaging the natural and forced convection Nusselt numbers from Eqs. (A.6) – (A.12) through the following empirical formula [11]:

$$Nu = \left[\left(Nu_{nc}\right)^3 + \left(Nu_{fc}\right)^3\right]^{1/3} \tag{A.13}$$

Once the average Nusselt number is determined, the outer convection heat transfer coefficient can be determined [10,11].

$$\overline{h}_o = Nu \cdot k_{fluid} / w \tag{A.14}$$

A.2.2 Convection heat transfer coefficient between skin and fabric

Similar dimensional analysis can be used to determine the inner convection heat transfer coefficient. It is assumed that the fabric is impermeable and, as such, no bulk flow exists in the space between the fabric and the skin. For the case of two vertically-oriented parallel plates, the convection coefficient will again depend on the Rayleigh number. In this case, the characteristic length is the gap between the parallel plates (b), as opposed to the plate width [10,11]:

$$Ra_b = Gr_b \cdot Pr = \frac{g b^3 \beta \left|T_{skin} - T_{fab}\right|}{\nu^2} \cdot Pr \tag{A.15}$$

The average Nusselt number and heat transfer coefficient will depend on the magnitude of the Ra_b compared to a critical Rayleigh number (Ra_{crit} = 1708). If $Ra_b \le Ra_{crit}$, the viscous dissipation forces of the fluid in the gap will outweigh buoyancy-driven forces. As a result, convection cannot be established and conduction is the dominant heat transfer mode across the gap (Nu=1). For $Ra_b > Ra_{crit}$, the Nusselt number will be greater than unity due to the presence of convective flows, but the appropriate correlation depends on the magnitude of Ra_b. The overall relations for various levels of Ra_b can be summarized as [11]:

$$Nu = 1 \qquad Ra_b \le 1708 \tag{A.16}$$

$$Nu = 0.42 Ra_b^{1/4} Pr^{0.012} \left(a/b\right)^{-0.3} \qquad 1708 < Ra_b \le 10^6 \tag{A.17}$$

$$Nu = 0.046 Ra_b^{1/3} \qquad 10^6 < Ra_b \le 10^9 \tag{A.18}$$

Once the average Nusselt number is determined from Eqs. (A.16) – (A.18), the average inner convection coefficient between the skin and the fabric can be determined [10,11]:

$$\overline{h}_i = Nu \cdot k_{fluid} / b \tag{A.19}$$

A.2.3 Determination of skin temperature

The human skin consists of the inner dermis and the outer epidermis, which are roughly 2 mm and 0.15 mm thick, respectively. The epidermis thermal conductivity ($k_{epidermis}$) is 0.21 W/m·K [14]. It is assumed that the dermis is maintained at the consistent temperature of 35°C due to vasoconstriction and vasodilation. However, it is necessary to account for the temperature drop across the epidermis where there is no blood vessel or capillary thermoregulation.

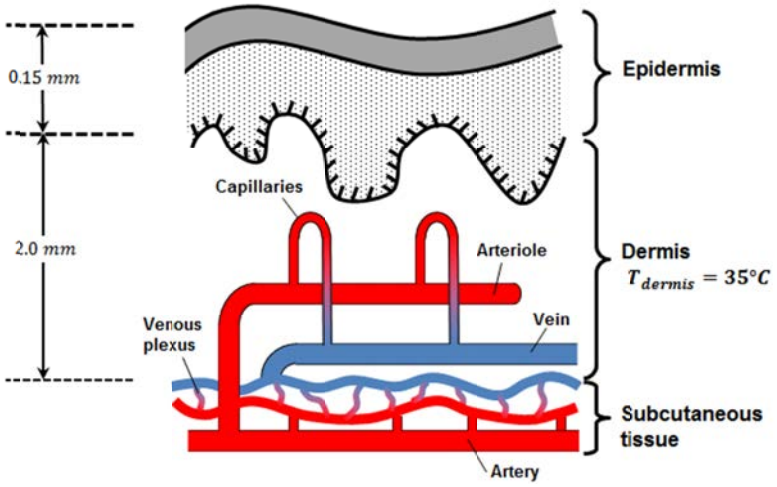

Fig. A-2. Skin vascular system (adapted from Guyton and Hall, 2000) [14].

The epidermis is modeled as a solid material experiencing one-dimensional, steady-state conduction. As such, the heat flow from the dermis must match the net heat leaving the skin towards the fabric ($Q_{loss,net} = Q_i + J_{sf} - J_{fs}$). Fourier's law of conduction then can be used to determine the temperature drop across the epidermis:

$$T_{skin} = T_{dermis} - \left[Q_i + J_{sf} - J_{fs} \right] \cdot t_{epidermis} / k_{epidermis} \tag{A.20}$$